IEEE Access
Multidisciplinary | Rapid Review | Open Access Journal

Received September 1, 2021, accepted September 9, 2021, date of publication September 17, 2021,
date of current version September 30, 2021.

Digital Object Identifier 10.1109/ACCESS.2021.3113712

Fractional-Slot PMSMs With One Coil Parallel Branches Made Phases–Part I: Investigation Study

AHMED MASMOUDI[1], (Senior Member, IEEE), SAHAR MKAOUAR[1], AICHA MAAOUI[1], AND MICHAEL SCHIER[2], (Member, IEEE)
[1]Laboratory of Renewable Energies and Electric Vehicles (RELEV), Sfax Engineering National School, University of Sfax, Sfax 3038, Tunisia
[2]Institute of Vehicle Concepts, German Aerospace Center, 70569 Stuttgart, Germany

Corresponding author: Ahmed Masmoudi (a.masmoudi@enis.rnu.tn)

ABSTRACT This work proposes an approach to design fractional-slot permanent magnet synchronous machines (FSPMSMs) equipped with phases made up of one coil parallel branches. These machines exhibit attractive potentialities, especially their enhanced open-circuit fault tolerance capability. Beyond their intrinsic fault tolerance, an open-circuit affecting the targeted topologies leads to a torque step-down limited to the one developed by the concerned coil rather than the torque produced by the total phase in FSPMSMs equipped with phases made up of series-connected coils. Furthermore, these topologies are suitably-adapted to low-voltage power supply that makes them viable candidates in automotive applications. This potentiality is by far vital in battery electric vehicles with the risk of electrocution in case of accident totally-eradicated thanks to the reduction of the DC bus voltage. Part 1 of the developed work is aimed at a star of slots-based identification and topological characterization of the FSPMSMs enabling the arrangement of the armature phases according to one coil parallel branches. The study distinguishes the topologies with odd and even number of phases, arranged in single- and double-layer slots. A case study is treated using a 2D finite element analysis and validated by experiments.

INDEX TERMS Fractional-slot permanent magnet synchronous machines, phases arranged in one coil parallel branches, start of slots approach, odd and even number of phases, single- and double-layer slots.

I. INTRODUCTION

Much attention is currently given to FSPMSMs to equip a variety of applications covering a wide range of power, from medical actuators and household appliances till wind turbines, going through electric and hybrid vehicles [1]–[5]. The great interest in FSPMSMs is motivated by [6]–[11]: (i) their low copper losses, (ii) their reduced cogging torque, (iii) their wide flux weakening range, and (iv) and their high fault tolerance capability thanks to their low mutual inductance. Further improvement of the fault tolerance is gained with the increase of the number of phases, yielding the so-called ''multi-phase FSPMSMs''. The design and post-fault feature recovery of multi-phase FSPMSMs have been widely reported in the literature. The most recent works are reviewed hereunder.

The associate editor coordinating the review of this manuscript and approving it for publication was Kan Liu.

In [12], *Qiao et al.* treated the design and analysis of a class of six-phase semi-symmetrical FSPMSMs aimed to ship propulsion application. A special attention has been paid to the investigation of the electromagnetic vibration caused by radial magnetic forces. In [13], *Liu* and *Zhu* introduced the magnetic gearing effect and the gear ratio in FSMPSMs, considering different number of phases and slot-pole combinations. The influence of the gear ratio on the winding factor, the output and cogging torques, the inductance, and the rotor loss of 3 and 6 phase FSPMSMs has been investigated and experimentally-validated. In [14], *Kuang et al.* considered a thermal analysis of a 10kw 28-pole 30-slot fifteen-phase FSPMSM drive under different faulty scenarios affecting the machine and the associated converter. Steady-state and transient thermal behaviors have been investigated by a finite element analysis and confirmed by experiments. In [15], *Gong et al.* treated the design of double polarity five-phase FSPMSMs developing the same torque either by the first or

the third current harmonic. In [16], *Harke* treated in detail the arrangement of six phase FSPMSMs. The possible slot-pole combinations have been discussed. Based on the star of slots approach, two winding arrangement techniques have been compared. An investigation of the fault tolerance highlighted the superiority of the design with two six phase belts. In [17], *Zhang et al.* considered the selection of the pole-slot combination and winding arrangement of a twelve-phase fractional-slot concentrated winding permanent magnet (PM) motor dedicated to ship propulsion. In [18], *Wu et al.* proposed a SiC-based integrated modular motor drive equipped with a five-phase FSPMSM. The motor and converter are cooled using a water jacket. A thermal analysis has been carried out with emphasis on the motor behavior, in order to improve the drive reliability at high-temperature operation. In [19], *Fan et al.* developed an approach to minimize the torque ripple caused by inter-turn short-circuit faults of a single-layer 20-slot IPM 18-pole 5-phase FSPMSM dedicated to electric vehicle application. In [20], *Scuiller et al.* treated the design and control of a seven-phase FSPMSM characterized by two fundamental harmonics. The so-called bi-harmonic design has been considered in an attempt to achieve a high torque density. In [21], *Huang et al.* considered the design 30-slot 24-pole 5-phase PMSM equipped with hybrid single/double layer fractional-slot concentrated winding applied to electric vehicles. A third harmonic current injection has been considered under healthy and faulty operations. In [22], *Zhao et al.* proposed a 20-slot 22-pole 5-phase outer rotor FSPMSM that exhibits a lower harmonic content of the air gap magnetomotive force compared to the conventional topology one. This has been achieved considering a star-pentagon connection of the 20 coils. In [23], *Huang et al.* proposed an equal-magnitude sinusoidal current compensation approach to improve the post-fault performance of a 10-slot 8-pole 5-phase FSPMSM under short-circuit faults. The proposed approach is based on the graphical rotating rhombus method. In [24], *Yin et al.* proposed a post-fault control strategy for a 10-slot, 8-pole 5-phase FSPMSM. Under a short-circuit fault, the d-axis armature magnetomotive force is changed from zero and the backward-rotating MMF components are kept null which enables the FSMPSM to recover a smooth torque. Finally, it should be underlined that a key step is required prior switching to any post-fault control strategy, that is the fault diagnosis [25]–[27].

An approach to improve the open-circuit fault tolerance has been proposed in [28]. It has the merit to be applicable to three and multi-phase machines. It consists in connecting in parallel the coils or suitable combinations of coils of each phase, so that in case of an open-circuit fault, only the concerned circuit turns to be passive rather than the total phase in series-connected coils. Furthermore, with their low-voltage power supply, FSPMSMs turn to be suitably-adapted to automotive applications. This approach has been extended to a class of FSPMSMs characterized by a star of slots including three phasors per phase and per winding period [29].

The approach introduced in [28] is deeply rethought in this work with emphasis on FSPMSMs equipped with one coil parallel branches made phases, considering:

1) both odd and even number of phases while only odd number of phases has been treated in [28],
2) a systematic identification allied to a topological characterisation of all candidates that makes it possible the phase arrangement according to one coil parallel branches, while limited number of slot-pole combinations have been considered in [28],
3) an investigation of the possible circulation of harmonic currents in the loops resulting from the parallel connection of the coils of each phase which affects the machine performance. Totally ignored in [28], this issue will be investigated in Part 2 of the present work.

II. IDENTIFICATION AND TOPOLOGICAL CHARACTERIZATION OF FSPMSMs WITH ONE COIL PARALLEL BRANCHES MADE PHASES

A. CASE OF ODD NUMBER OF PHASES

This case is characterized by a star of slots with the back-EMF phasors, induced in the coils of a given phase, aligned in one or the two opposite sectors assigned to that phase.

1) CASE OF DOUBLE-LAYER SLOTS

Let us call N_s the number of slots in the stator, p the number of pole pairs in the rotor, and q the number of phases. Odd and even fundamental back-EMF phasors are successively-shifted in the star of slots by an angle $\alpha_p = p\frac{2\pi}{N_s}$.

The case where the FSPMSM phases are made up of one coil parallel branches, is achieved when the star of slots fulfills the following criteria:

- Case 1: all back-EMF phasors assigned to a phase are aligned in one sector as illustrated in Fig. 1. This case covers both even and odd number of coils N_s, with:

$$\alpha_p = \begin{cases} \left(\frac{q-1}{q}\right)\pi & Fig.\ 1(a) \\ \left(\frac{q+1}{q}\right)\pi & Fig.\ 1(b) \end{cases} \tag{1}$$

  The winding factor K_{wp}^{dl} is obtained from Fig. 1 as:

$$K_{wp}^{dl} = \frac{2E\cos\left(\frac{\pi}{2q}\right)}{2E} = \cos\left(\frac{\pi}{2q}\right) \tag{2}$$

  where E is the amplitude of the coil back-EMF phasor.
- Case 2: the back-EMF phasors assigned to a phase are aligned and equally-distributed in the two opposite sectors, as shown in Fig. 2. This case is only feasible with an even number of coils N_s, with:

$$\alpha_p = \begin{cases} \left(\frac{2q-1}{q}\right)\pi & Fig.\ 2(a) \\ \left(\frac{2q+1}{q}\right)\pi & Fig.\ 2(b) \end{cases} \tag{3}$$

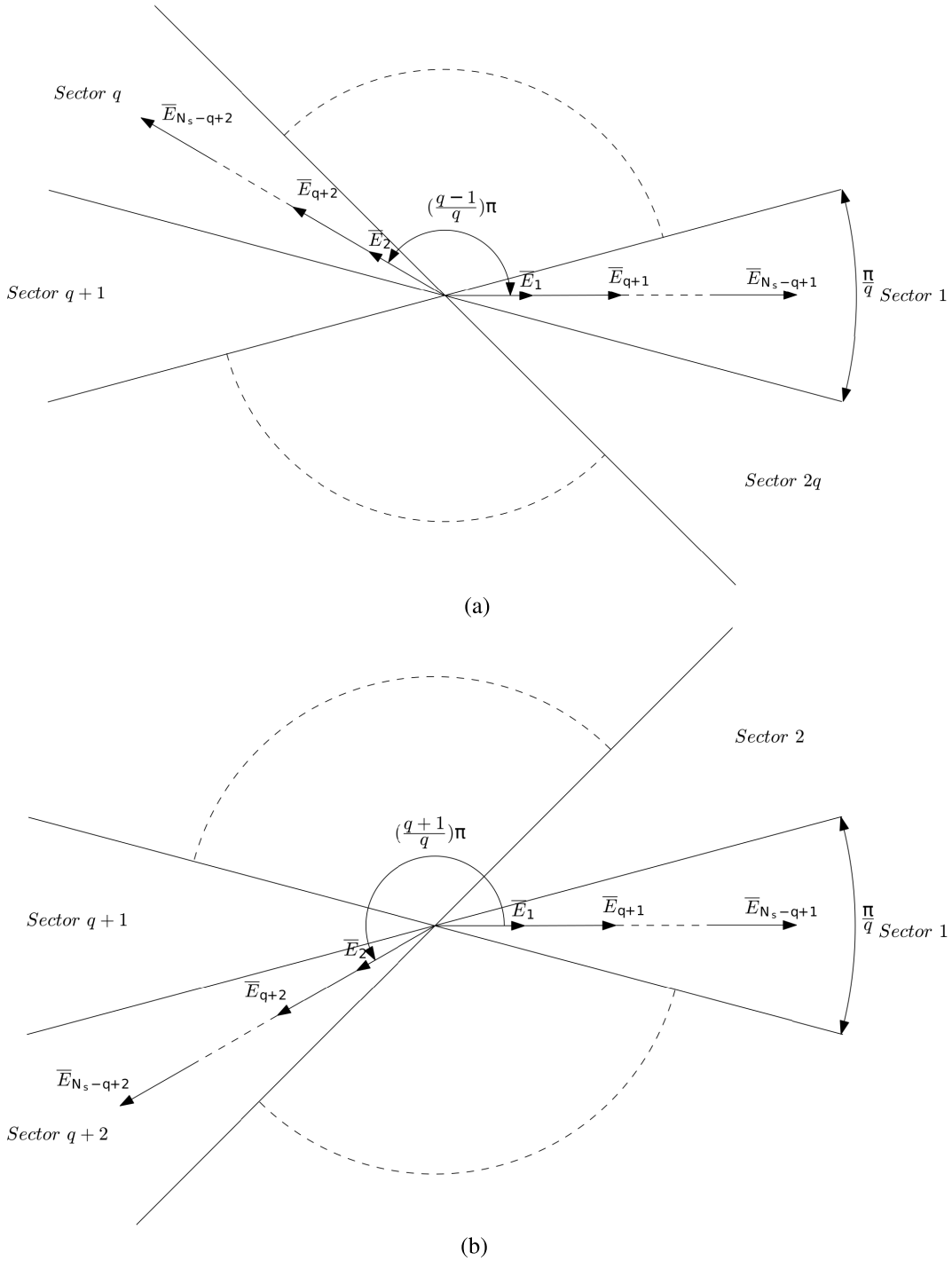

FIGURE 1. Star of slots of the FSPMSMs with odd number of phases arranged in double-layer slots in the case where all phase back-EMF phasors are aligned in one sector among the two sectors assigned to the phase. **Legend: (a) two successive back-EMFs shifted by $(\frac{q-1}{q})\pi$, (b) two successive back-EMFs shifted by $(\frac{q+1}{q})\pi$.**

Referring to Fig. 2, K_{wp}^{dl} is expressed as follows:

$$K_{wp}^{dl} = \frac{2E\cos\left(\frac{(q-1)\pi}{2q}\right)}{2E} = \sin\left(\frac{\pi}{2q}\right) \tag{4}$$

The parallel connection of the coils of a phase in both cases is illustrated in Fig. 3. Referring to equations (2) and (4), one can clearly notice that the FSPMSMs characterized by the star of slots of Fig. 1 exhibit interesting K_{wp}^{dl}. Three phase candidates, characterized by their slot-pole combinations, have been identified in [28]. While the candidates characterized by the star of slots of Fig. 2 are penalized by

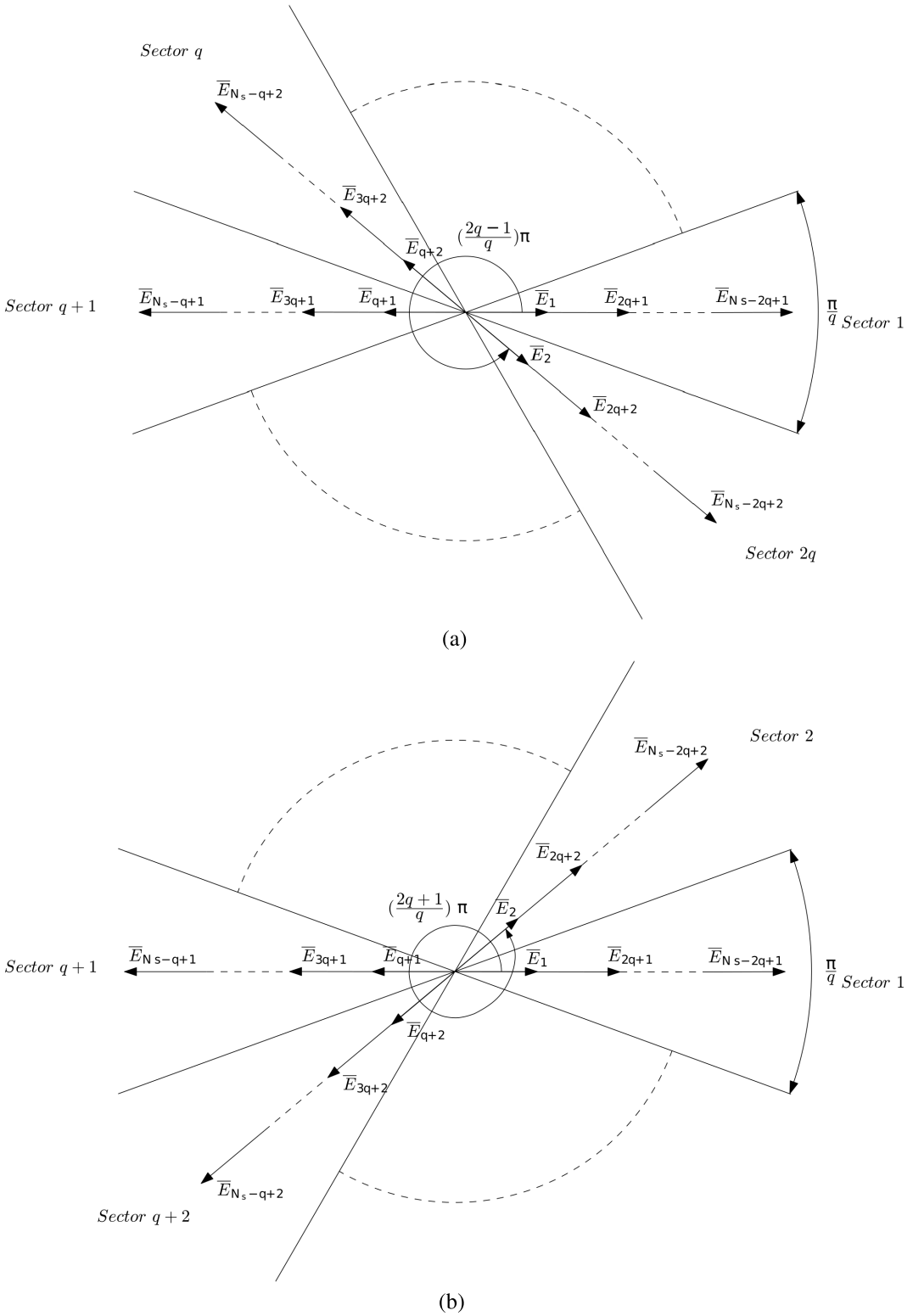

FIGURE 2. Star of slots of FSPMSMs with odd number of phases arranged in double-layer slots in the case where the phase back-EMF phasors are aligned and equally-distributed in the two opposite sectors assigned to the phase. **Legend: (a) two successive back-EMF phasors shifted by $(\frac{2q-1}{q})\,\pi$, (b) two successive back-EMF phasors shifted by $(\frac{2q+1}{q})\,\pi$.**

their low fundamental winding factors. The slot-pole combinations of three phase machines are identified in table 1.

2) CASE OF SINGLE-LAYER SLOTS

The star of slots enabling the arrangement of the coils in single-layer slots is deduced form the double-layer slots one

TABLE 1. Slot-pole combinations for $q = 3$ in the case of double-layer slots with the back-EMF phasors of a phase co-linear equally-distributed in the two opposite sectors in the star of slots. **Legend:** dark-blue: slot per pole and per phase $S_{pp} = \frac{1}{5}$, orange: $S_{pp} = \frac{1}{7}$, pink: $S_{pp} = \frac{1}{11}$, gray: $S_{pp} = \frac{1}{13}$, purple: $S_{pp} = \frac{1}{17}$, green: $S_{pp} = \frac{1}{19}$, light-blue: $S_{pp} = \frac{1}{23}$, yellow: $S_{pp} = \frac{1}{25}$, red: $S_{pp} = \frac{1}{29}$, blue: $S_{pp} = \frac{1}{31}$, turquoise: $S_{pp} = \frac{1}{35}$, light-green: $S_{pp} = \frac{1}{37}$.

N_s \ p	2	3	4	5	6	7	8	9	10	11	12	13	14	15	16	17	18	19	20	21	22	23	24	25	26	27	28	29	30	31	32	33	34	35	36	37	38	39	40
6																																								
12																																							
18																																							
24																																							
30																																							
36																																							

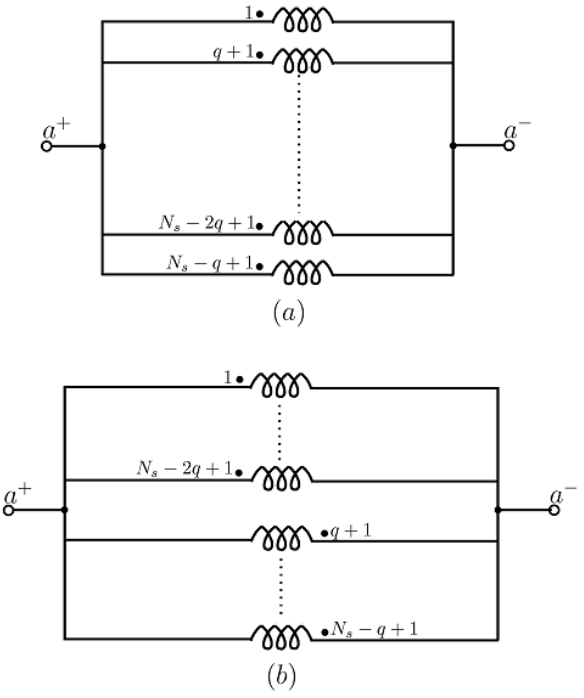

FIGURE 3. Parallel Connection of the coils of a phase. **Legend:** (a) case of Fig. 1, (b) case of Fig. 2.

by removing the even back-EMF phasors. In order to arrange the phases in one coil parallel branches, this approach has been applied to the star of slots of Figs. 1 and 2.

A second approach to arrange the phases in single-layer slots is proposed in this work. It consists in removing a spoke of aligned even back-EMF phasor(s) from each sector of the star of slots corresponding to the double-layer slots. This latter includes two spokes of back-EMF phasor(s) per sector, such that:

- the ones made up of even back-EMF phasor(s) are co-linear and located in the two opposite sectors,
- the ones made up of odd back-EMF phasor(s) are co-linear and located in the two opposite sectors.

as depicted in the star of slots of Fig. 4.

Following the removal of the even back-EMF phasors from the star of slots of Figs. 1 and 2, the resulting winding factors in the case of single-layer slots, noted K_{wp}^{sl}, are similar to the ones in the case of double-layer slots K_{wp}^{dl}. Considering the second approach, Fig. 4 enables the prediction of K_{wp}^{sl} as:

$$K_{wp}^{sl} = \frac{2E\cos\left(\frac{\pi}{2} - \frac{(2q-1)\pi}{4q}\right)}{2E} = \cos\left(\frac{\pi}{4q}\right) \quad (5)$$

It is to be noted that, for a given number of phases, the second approach exhibits a higher K_{wp}^{sl} than those given by expressions (2) and (4).

B. CASE OF EVEN NUMBER OF PHASES

It should be underlined that the star of slots in the case of even number of phases differs from the one in the case of odd number of phases, by the localisation of the two sectors assigned to a phase, such that:

- in the case of odd number of phases, the two sectors are shifted by π,
- in the case of even number of phases, the two sectors are shifted by $\left(\pi + \frac{\pi}{q}\right)$ [30].

1) CASE OF DOUBLE-LAYER SLOTS

Arranging the phases according to one coil parallel branches inserted in double-layer slots is feasible if the tow following conditions are fulfilled:

- all phase back-EMF vectors are located in one sector,
- the angular shift between two adjacent back-EMF phasors is equal to the electrical shift between two adjacent phases ($\alpha_p = \frac{2\pi}{q}$),

as shown in Fig. 5. This latter enables a graphical determination of the fundamental back-EMF winding factor K_{wp}^{dl}, as:

$$K_{wp}^{dl} = \frac{2E\cos\left(\frac{\pi}{2} - \frac{\pi}{q}\right)}{2E} = \sin\frac{\pi}{q} \quad (6)$$

The slot-pole combinations enabling the arrangement of the phases according to one coil parallel branches in the case of $q = 4$ and $q = 6$ are identified in tables 2 and 3, respectively.

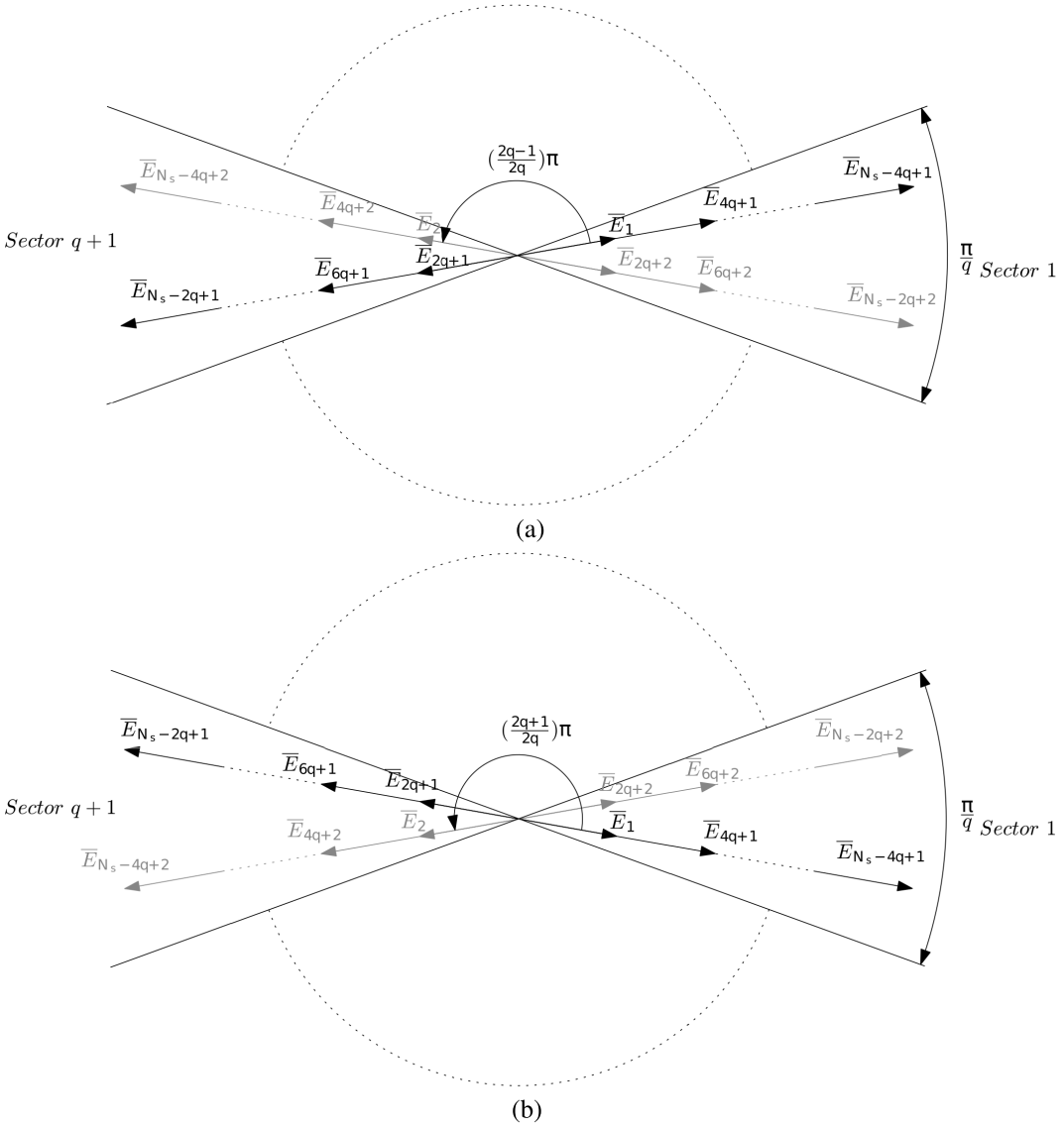

FIGURE 4. Star of slots of FSPMSMs fulfilling the second approach to arrange one coil parallel branches made armature phases in single-layer slots. **Legend 1:** (a) $\alpha_p = (\frac{2q-1}{2q})\,\pi$. (b) $\alpha_p = (\frac{2q+1}{2q})\,\pi$. **Legend 2:** (black): back-EMF phasors of the coils inserted in single-layer slots, (gray): back-EMF phasors drawn assuming double-layer slots prior their removal.

2) CASE OF SINGLE-LAYER SLOTS

The removal of the even back-EMF phasors from the star of slots of Fig. 5, leads to the coil arrangement in single-layer slots. The resulting winding factor K_{wp}^{sl} is similar to one given by expression (6).

A second approach that makes it possible the arrangement of one coil parallel branches in single-layer slots, is proposed. It is characterized by the star of slots of Fig. 6 from which one can predict K_{wp}^{sl} as:

$$K_{wp}^{sl} = \cos(\frac{\pi}{2q}) \tag{7}$$

It is to be noted that, for a given number of phases, the second approach leads to a higher K_{wp}^{sl} than the one yielded by expression (6). The possible slot-pole combinations, characterizing the cases of $q = 4$ and $q = 6$ arranged in single-layer slots, are regrouped in tables 4 and 5, respectively.

III. CASE STUDY

A. TOPOLOGICAL DESCRIPTION

The FSPMSM under study is characterized by:

- a number of phases $q = 3$,
- a number of double-layer slots $N_s = 18$,
- a number of pole pairs $p = 6$ achieved by interior PMs. A pole is made up of two PM rows incorporating 15 axial

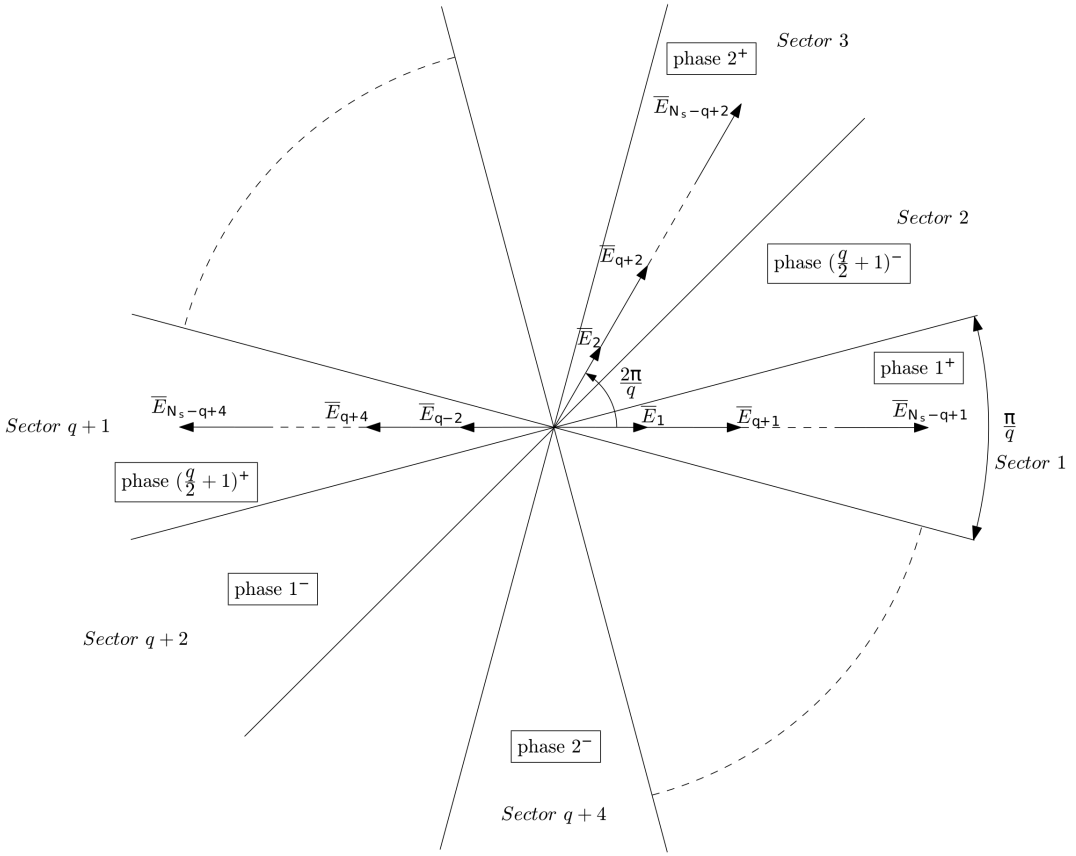

FIGURE 5. Star of slots of FSPMSMs with even number of phases arranged in double-layer slots.

TABLE 2. Slot-pole combinations for $q = 6$ and double-layer slots. Legend: dark-blue $S_{pp} = \frac{1}{2}$, light-blue $S_{pp} = \frac{1}{14}$, pink $S_{pp} = \frac{1}{26}$, gray $S_{pp} = \frac{1}{38}$.

N_s \ p	2	3	4	5	6	7	8	9	10	11	12	13	14	15	16	17	18	19	20	21	22	23	24	25	26	27	28	29	30	31	32	33	34	35	36	37	38	39	40
8																																								
12																																								
16																																								
20																																								
24																																								
28																																								
32																																								
36																																								

TABLE 3. Slot-pole combinations for $q = 6$ and double-layer slots. Legend: dark-blue $S_{pp} = \frac{1}{2}$, light-blue $S_{pp} = \frac{1}{14}$, pink $S_{pp} = \frac{1}{26}$, gray $S_{pp} = \frac{1}{38}$.

N_s \ p	2	3	4	5	6	7	8	9	10	11	12	13	14	15	16	17	18	19	20	21	22	23	24	25	26	27	28	29	30	31	32	33	34	35	36	37	38	39	40
12																																								
18																																								
24																																								
30																																								
36																																								

segments each. The pole segmentation has been considered in order to reduced the PM eddy current loss caused by the dense harmonic content of the armature magnetic reaction [27]–[31].

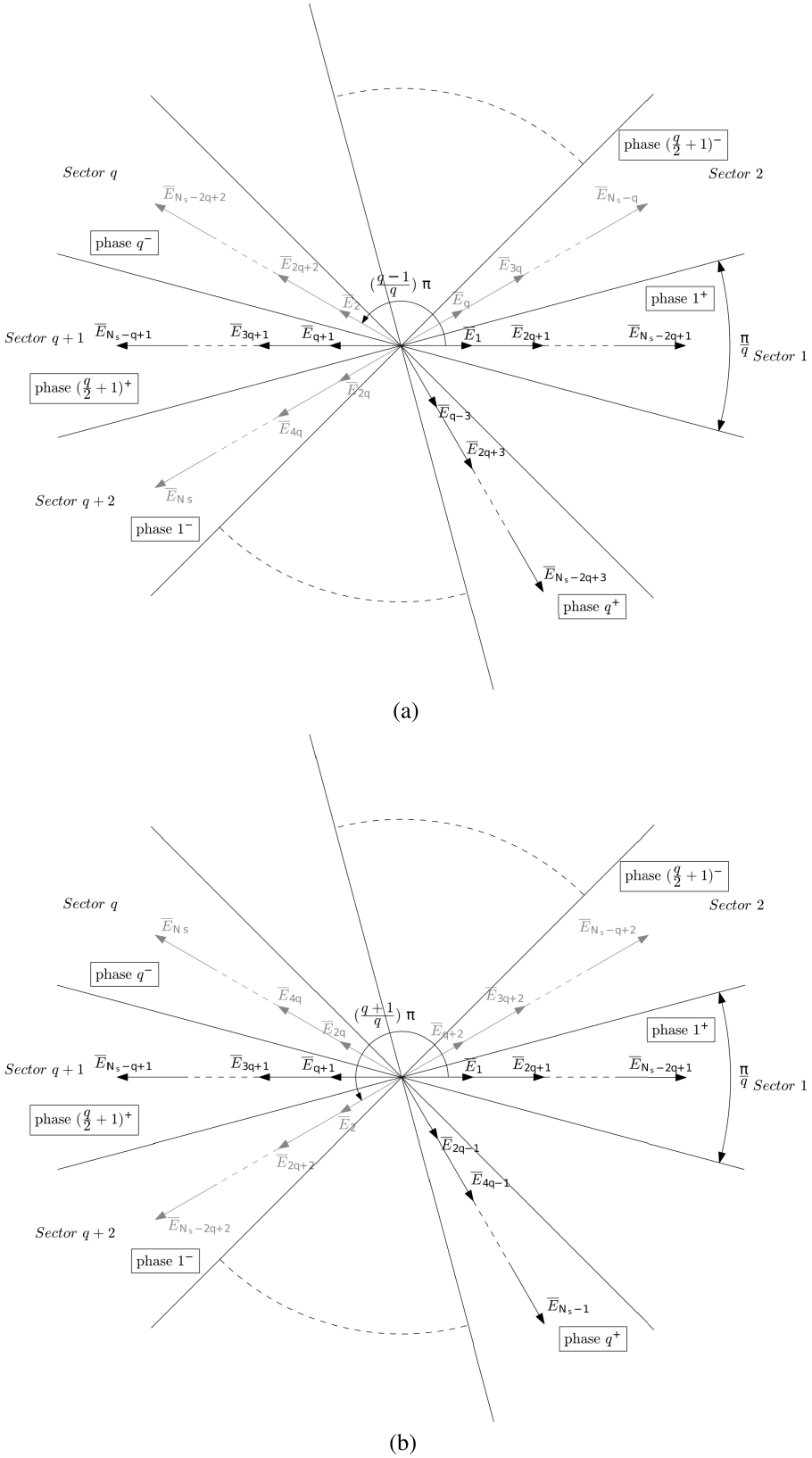

FIGURE 6. Star of slots of FSPMSMs equipped with an even number of phases made up of one coil parallel branches arranged in single-layer slots. **Legend 1:** (black): back-EMF phasors of the coils inserted in single-layer slots, (gray) back-EMF phasors removed in the case of single-layer slots. **Legend 2:** (a) $\alpha_p = (\frac{q-1}{q})\,\pi$. (b) $\alpha_p = (\frac{q+1}{q})\,\pi$.

TABLE 4. Slot-pole combinations for $q = 6$ in the case of single-layer slots. **Legend 1: colored boxes given by the first approach with: dark-blue $S_{pp} = \frac{1}{2}$, light-blue $S_{pp} = \frac{1}{14}$, pink $S_{pp} = \frac{1}{26}$, gray $S_{pp} = \frac{1}{38}$. Legend 2: hatched boxes given by the second approach with: turquoise $S_{pp} = \frac{1}{5}$, red $S_{pp} = \frac{1}{7}$, yellow $S_{pp} = \frac{1}{17}$, purple $S_{pp} = \frac{1}{19}$, green $S_{pp} = \frac{1}{29}$, orange $S_{pp} = \frac{1}{31}$.**

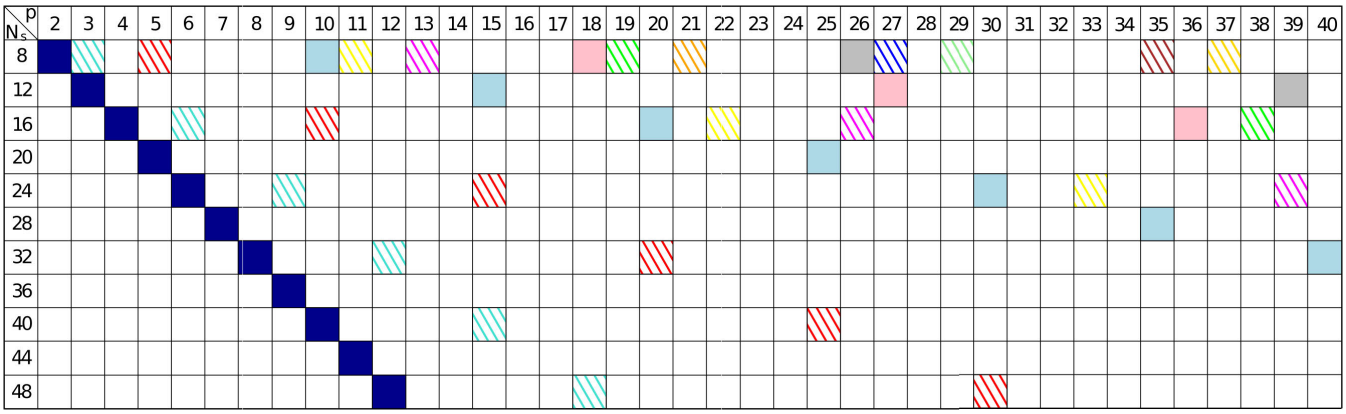

TABLE 5. Slot-pole combinations for $q = 6$ in the case of single-layer slots. **Legend 1: colored boxes given by the first approach with: dark-blue $S_{pp} = \frac{1}{2}$, light-blue $S_{pp} = \frac{1}{14}$, pink $S_{pp} = \frac{1}{26}$, gray $S_{pp} = \frac{1}{38}$. Legend 2: hatched boxes given by the second approach with: turquoise $S_{pp} = \frac{1}{5}$, red $S_{pp} = \frac{1}{7}$, yellow $S_{pp} = \frac{1}{17}$, purple $S_{pp} = \frac{1}{19}$, green $S_{pp} = \frac{1}{29}$, orange $S_{pp} = \frac{1}{31}$.**

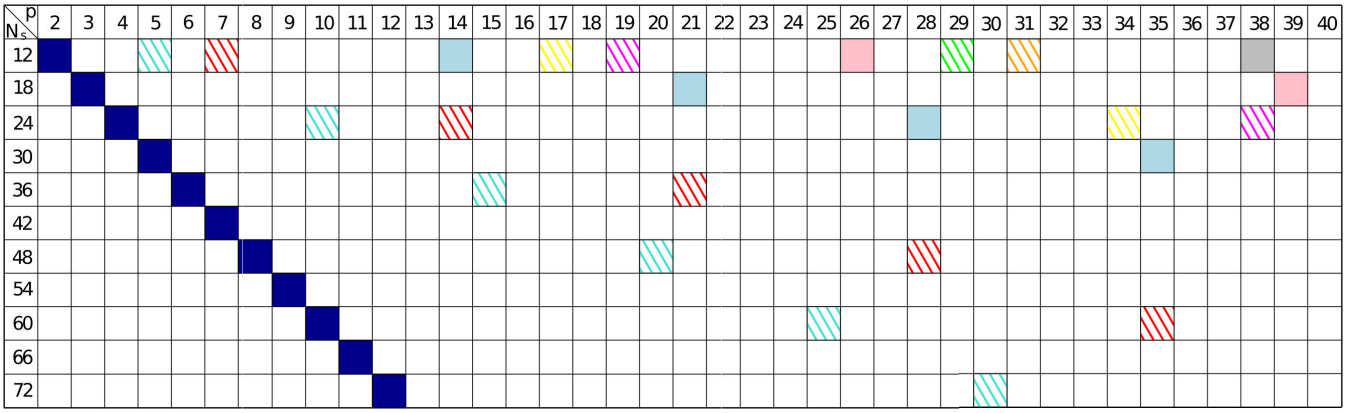

It has the star of slots depicted in Fig. 7, resulting in a fundamental winding factor $K_{wp}^{dl} = \sqrt{3}/2 \simeq 0.866$. It belongs to FSPMSM class characterized by the star of slots of Fig. 1(a). Thus, in the case of one coil open-circuit faulty scenario, the machine would lose 1/18 of its torque production capability. However, considering a series connection of its coils, in the case of one coil open-circuit faulty scenario, the machine would lose 1/3 of its torque production capability along with a high torque ripple. A quarter of the machine cross-section is shown in Fig. 8 where the main geometrical parameters are identified. These are listed in table 6.

The iron parts of the magnetic circuit are made up of M270/35A. The permanent magnets are made up of rare earth NdFeB with a remanence of 1.1T and a cœrcitivity of -875352.187A/m. The total mass of the PMs is 2.736kg. The masses of the stator and rotor cores are 22,3kg and 12,5kg, respectively. The mass of the shaft is 5.8kg. The mass of the remaining parts of the rotor is 2.744kg. The copper mass is 1.719kg with 95.5g per coil. The slot fill factor is 0.3. The winding wire diameter is 0,94mm. The number of conductors per slot is 80.

B. PREDICTION OF THE NO-LOAD FEATURES

The no-load flux density mapping and lines throughout the study domain have been computed by a 2D FEA. The obtained results are shown in Figs 9 and 10, respectively. One can notice that the flux density can reach a maximum of 2.3T, causing a local saturation in the rotor iron areas facing the PMs' edges close to the air gap as well as in the space separating the two pole PM pieces.

Fig. 11 shows the no-load air gap flux density over a pole pair with a maximum value not exceeding 0.6T. Such a low value results from a remarkable pole edge leakage flux, as confirmed by the flux lines shown in Fig. 10. This drawback is due to a mis-sized PM length and does not have any link with the arrangement of the phases according to one coil parallel branches. This statement will be clearly demonstrated in paragraph III-D. Moreover, it is to be noted that the south pole is affected by a remarkable spike which is caused by the slotting effect.

Fig. 12 shows the waveform of the phase back-EMFs of the FSPMSM under study for the base speed 2600rpm. One can notice that the back-EMFs are not sinusoidal. In case

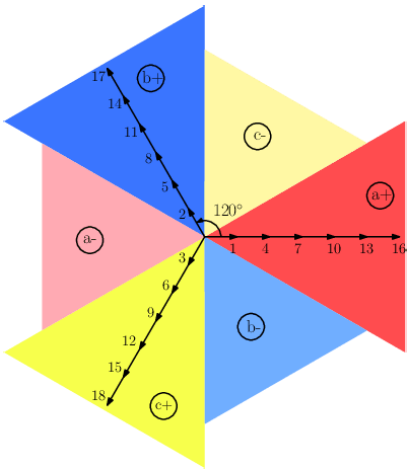

FIGURE 7. Star of slots of the FSPMSM under study, characterized by $q = 3$, $N_s = 18$, $p = 6$.

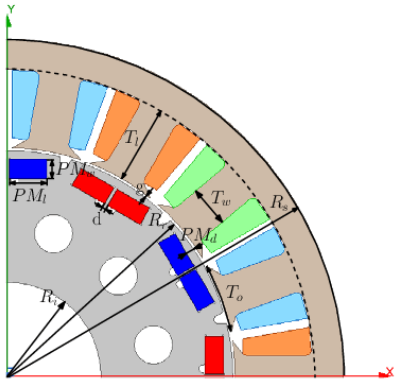

FIGURE 8. FSPMSM under study: quarter of the cross section.

TABLE 6. FSPMSM under study: geometrical parameters.

Parameter	Symbol	Value (mm)
PM width	PM_w	5
PM segment length	PM_l	10
PM segment axial length	PM_a	20
Distance between the two PM segments	d	0.8
PM depth	PM_d	2
Rotor inner radius	R_i	25
Rotor outer radius	R_r	60.3
Air gap thickness	g	0.7
Stator outer radius	R_s	90
Stator yoke width	Y_w	8
Teeth width	T_w	11
Teeth opening	T_o	18.9
Teeth length	T_l	21
Slot opening	S_o	3
Active length	L_a	300

the harmonics of the back-EMFs induced in the parallel branches of a given phase are not in phase, this would lead to circulating harmonic currents, resulting in a degradation of the machine performance. Part 2 of this work will be dedicated to the investigation of the possibility that FSPMSMs, with their phases arranged in one coil parallel branches, may be penalized by circulating harmonic currents.

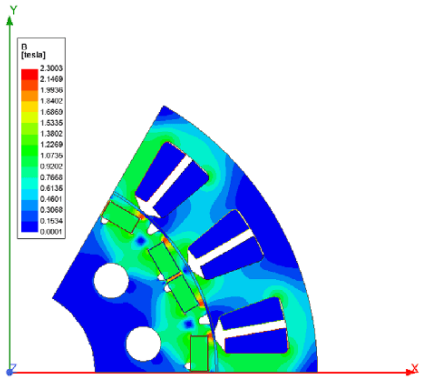

FIGURE 9. Flux density mapping at no-load operation.

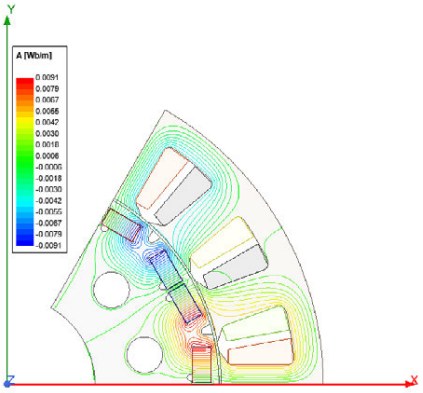

FIGURE 10. Flux lines at no-load operation.

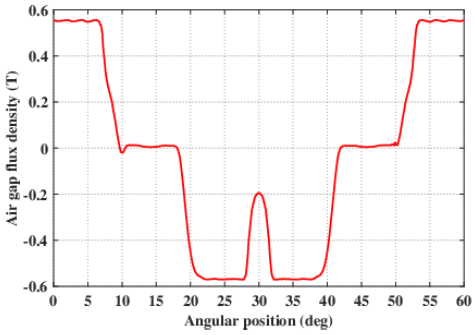

FIGURE 11. Air gap flux density over a pole pair.

C. EXPERIMENTAL VALIDATION

The topology described and investigated by FEA in the two previous paragraphs has been prototyped. Photos of the stator and rotor ((b) assembled and (c) PMs and shaft dismantled) are shown in Fig. 13. It has been developed at the German Aerospace Center within a project aimed at the design and performance assessment of a two-in-one-motor system. This latter is made up two FSPMSMs mechanically-coupled by an electromagnetic clutch. A photo of the developed test bench is shown in Fig. 14 where EM1 is the FSPMSM under study.

The back-EMF has been measured for a speed almost equal to 480rpm whose scope capture is shown in Fig. 15.

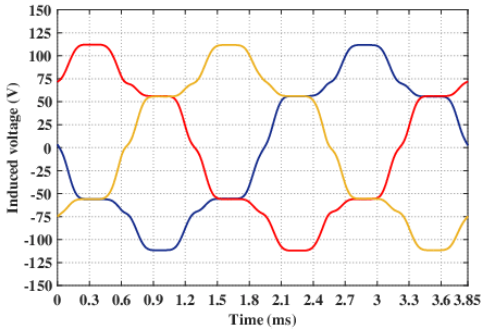

FIGURE 12. Phase back-EMFs for a speed of 2600rpm.

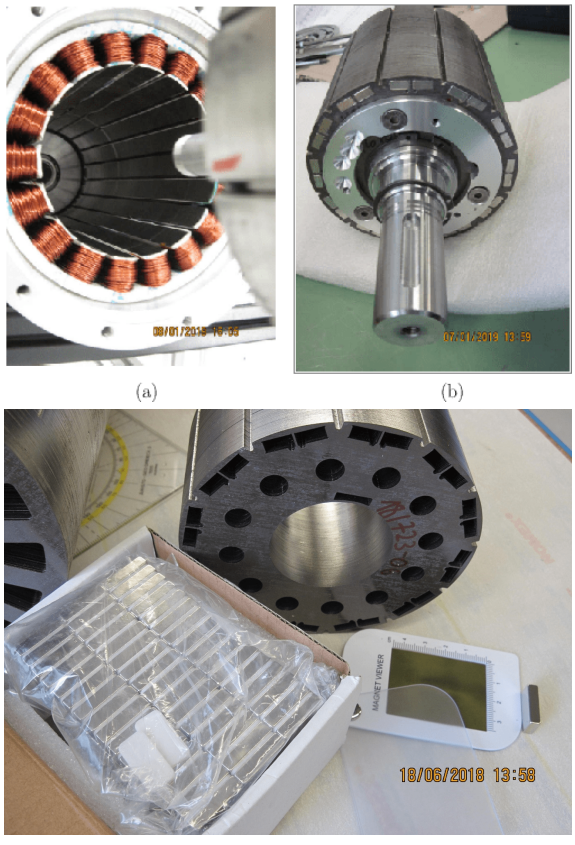

FIGURE 13. Prototyped FSPMSM. **Legend:** (a): stator, (b) rotor, (c) rotor iron and box containing the PM segments.

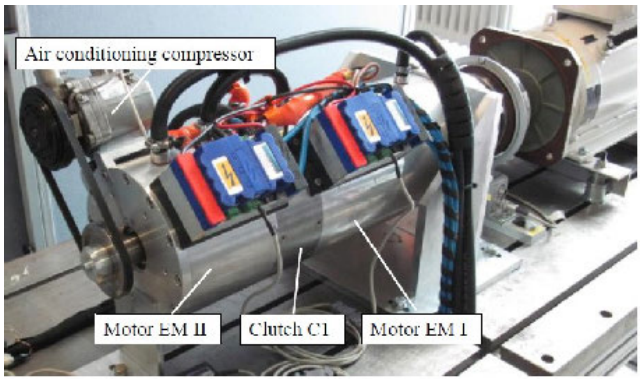

FIGURE 14. Test bench of the two-in-one-motor system.

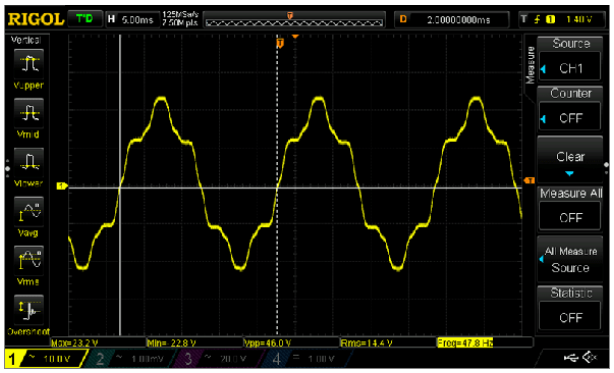

FIGURE 15. Back-EMF measured for a speed $N \simeq 480$rpm.

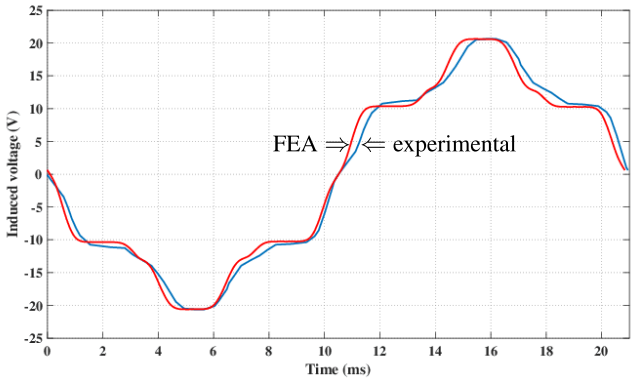

FIGURE 16. Back-EMF waveform of the prototyped FSPMSM for a speed almost equal to 480rpm. **Legend:** (red): FEA results, (blue): experimental data.

One can remark that the back-EMF has a waveform similar to the one shown in Fig. 12 with a peak-to-peak value of 46V. The back-EMF has been also predicted by FEA considering the same speed. Fig. 16 shows a single-period waveform of the measured and FEA-predicted back-EMFs. A quite acceptable agreement has been noticed. Further experimental results are provided and discussed in Part 2 of this work.

D. DESIGN IMPROVEMENT

As previously underlined in paragraph III-B, the prototyped machine suffers from a remarkable pole edge leakage flux due to a mis-sized PM segment length PM_l. A FEA-based investigation of its influence on the no-load features has been carried out considering the flowchart illustrated in Fig 17. It has been found that an increase of PM_l from 10mm to 12mm leads to a significant improvement of the no-load features as depicted in Figs. 18 to 21.

Following the comparison of the flux lines shown in Figs. 10 and 18, it has been noticed that the pole edge leakage flux has been remarkably reduced. As expected, this improvement has a direct positive impact on the air gap flux

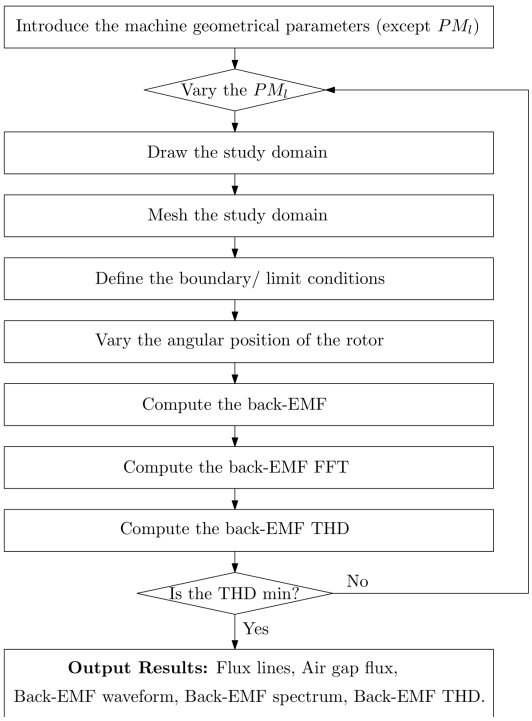

FIGURE 17. Flowchart of the developed FEA procedure that enabled the investigation of the effect of PM_l on the no-load features.

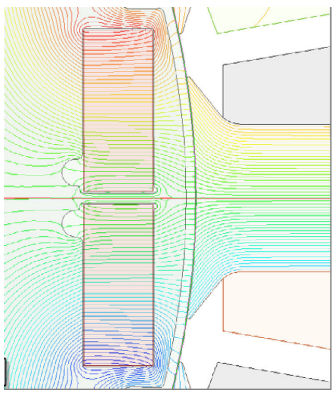

FIGURE 18. Zoom view of the flux lines for $PM_l = 12$mm.

density waveform, as illustrated in Fig. 19. For the sake of comparison, the air gap flux density waveform illustrated in Fig. 11 is recalled in Fig. 19 (dashed line).

The investigation has been extended to the back-EMF waveform and has led to the results shown in Fig. 20. Compared to the back-EMF waveform depicted in Fig. 12, one can notice an improvement in both amplitude and harmonic content. This statement is confirmed by the spectra of Fig. 21, corresponding to the FFT of the back-EMFs illustrated in Figs. 12 and 20 where the amplitudes have been normalised to the one of the fundamental in the case of $PM_l = 12$mm.

From the spectra of Fig. 21, one can notice that, following the increase of PM_l from 10mm to 12mm, the back-EMF waveform turns to be more sinusoidal with a remarkable:

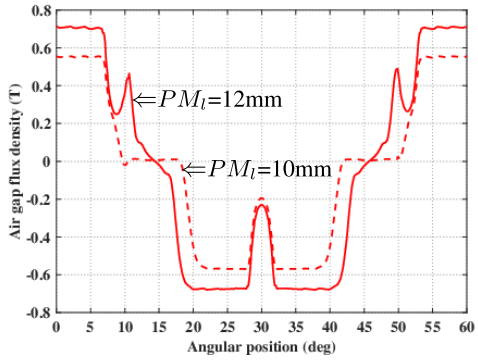

FIGURE 19. Air gap flux density waveform. **Legend:** (continuous line): $PM_l = 12$mm, (dashed line): $PM_l = 10$mm.

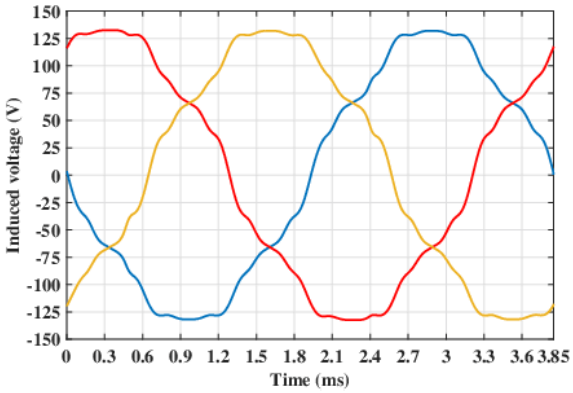

FIGURE 20. Back-EMF for $PM_l = 12$mm and a speed of 2600rpm.

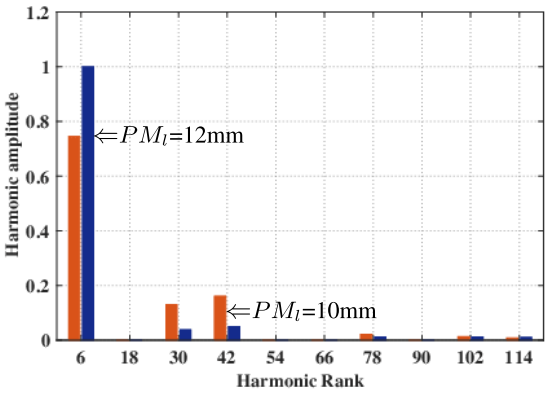

FIGURE 21. Back-EMF Spectra with normalised amplitudes. **Legend:** (blue): $PM_l = 12$mm, (orange): $PM_l = 10$mm.

- increase of 34.28% in the amplitude of the fundamental,
- decrease of 70.77% in the amplitude of the harmonic of rank 5,
- decrease of 68.94% in the amplitude of the harmonic of rank 7.

The resulting reduction of the harmonic content is characterized by an amelioration of the THD, such that:

$$THD \simeq \begin{cases} 13\% & for\ L_{PM} = 12mm \\ 21\% & for\ L_{PM} = 10mm \end{cases}$$

The great interest in the reduction of the harmonic content is motivated by the risk that the back-EMF harmonics may generate circulating harmonic currents in the parallel branches. The investigation of this risk will be treated in Part 2.

IV. CONCLUSION

This work investigated a class of FSPMSMs that make it possible the arrangement of their phases within one coil parallel branches. These are reputed by their enhanced open-circuit fault tolerance capability. Part 1 of the work developed a star of slots-based approach aimed at the identification and the topological characterization of all candidates which belong to the above-described class of FSPMSMs. This has been achieved considering the cases of odd and even number of phases, arranged in single- and double-layer slots. The identified candidates have been systematically-characterized by their winding factors and their slot-pole combinations.

It has been found that the identified candidates with their armature arranged in single-layer slots exhibit higher winding factors than their counterparts arranged in double-layer slots. Of particular interest are the candidates equipped with odd number of phases whose double-layer star of slots, prior the removal of even back-EMF phasors, are characterized by two spokes in each sector. These are expected to exhibit the highest torque production capability.

A case study has been treated considering a FSPMSM equipped with three phases in the armature having six parallel branches of one coil each. A 2D FEA-based investigation of its no-load features has revealed a remarkable pole edge leakage flux. It also enabled the prediction of the back-EMF which has been experimentally-validated. The paper has been achieved by a FEA-based resizing of the PM length aimed at the minimization of the pole edge leakage flux, thanks to which a reduction of the back-EMF harmonic content has been gained.

Prior to go in depth in the modelling and control of the identified candidates, especially the synthesis of dedicated post-fault strategies, an investigation of the possible circulation of harmonic currents in the loops resulting from the parallel connection of the phase coils is a mandatory step. Part 2 of this work develops this idea.

REFERENCES

[1] F. Wang, Y. Zhu, H. Wang, and D. Zhao, "Design and analysis of a bearingless permanent-magnet motor for axial blood pump applications," *IEEE Access*, vol. 8, pp. 7622–7627, 2021.

[2] O. Payza, Y. Demir, and M. Aydin, "Investigation of losses for a concentrated winding high-speed permanent magnet-assisted synchronous reluctance motor for washing machine application," *IEEE Trans. Magn.*, vol. 54, no. 11, pp. 1–5, Nov. 2018.

[3] W. Gul, Q. Gao, and W. Lenwari, "Optimal design of a 5-MW double-stator single-rotor PMSG for offshore direct drive wind turbines," *IEEE Trans. Ind. Appl.*, vol. 56, no. 1, pp. 216–225, Jan. 2020.

[4] C. Zhou, X. Huang, Z. Li, and W. Cao, "Design consideration of fractional slot concentrated winding interior permanent magnet synchronous motor for EV and HEV applications," *IEEE Access*, vol. 9, pp. 64116–64126, 2021.

[5] M. Y. Metwly, M. S. Abdel-Majeed, A. S. Abdel-Khalik, R. A. Hamdy, M. S. Hamad, and S. Ahmed, "A review of integrated on-board EV battery chargers: Advanced topologies, recent developments and optimal selection of FSCW slot/pole combination," *IEEE Access*, vol. 8, pp. 85216–85242, 2020.

[6] A. M. EL-Refaie, "Fractional-slot concentrated-windings synchronous permanent magnet machines: Opportunities and challenges," *IEEE Trans. Ind. Electron.*, vol. 57, no. 1, pp. 107–121, Sep. 2010.

[7] E. Fornasiero, L. Alberti, N. Bianchi, and S. Bolognani, "Considerations on selecting fractional-slot nonoverlapped coil windings," *IEEE Trans. Ind. Appl.*, vol. 49, no. 3, pp. 1316–1324, May/Jun. 2013.

[8] P. Ponomarev, Y. Alexandrova, I. Petrov, P. Lindh, E. Lomonova, and J. Pyrhonen, "Inductance calculation of tooth-coil permanent-magnet synchronous machines," *IEEE Trans. Ind. Electron.*, vol. 61, no. 11, pp. 5966–5973, Nov. 2014.

[9] Z. Zhu, Y. Huang, J. Dong, and F. Peng, "Investigation study of the influence of pole numbers on torque density and flux-weakening ability of fractional slot concentrated winding wheel-hub machines," *IEEE Access*, vol. 7, pp. 84918–84928, 2019.

[10] F. Chai, L. Geng, and Y. Pei, "A novel fault tolerant machine with integral slot non-overlapping concentrated winding," *IEEE Access*, vol. 7, pp. 2169–3536, 2019.

[11] H. Qu and Z. Q. Zhu, "Comparative study of electromagnetic performance of stator slot PM machines," *IEEE Access*, vol. 9, pp. 41876–41890, 2021.

[12] M. Qiao, C. Jiang, Y. Zhu, and G. Li, "Research on design method and electromagnetic vibration of six-phase fractional-slot concentrated-winding PM motor suitable for ship propulsion," *IEEE Access*, vol. 4, pp. 8535–8543, 2016.

[13] Y. Liu and Z. Q. Zhu, "Influence of gear ratio on the performance of fractional slot concentrated winding permanent magnet machines," *IEEE Trans. Ind. Electron.*, vol. 66, no. 10, pp. 7593-7602, Dec. 2019.

[14] Z. Kuang, S. Wu, B. Du, H. Xu, S. Cui, and C. C. Chan, "Thermal analysis of fifteen-phase permanent magnet synchronous motor under different fault tolerant operations," *IEEE Access*, vol. 7, pp. 81466–81480, 2019.

[15] J. Gong, H. Zahr, E. Semail, M. Trabelsi, B. Aslan, and F. Scuiller, "Design considerations of five-phase machine with double p/3p polarity," *IEEE Trans. Energy Convers.*, vol. 34, no. 1, pp. 12–24, Mar. 2019.

[16] M. Harke, "Design of fractional slot windings with coil span of two slots for use in six-phase synchronous machines," *J. Eng.*, vol. 2019, no. 17, pp. 4391–4395, Jun. 2019.

[17] B. Zhang, B. Du, T. Zhao, and S. Cui, "Research on the combinations of pole and slot for twelve-phase fractional-slot concentrated-winding permanent magnet motor," in *Proc. 22nd Int. Conf. Electr. Mach. Syst. (ICEMS)*, Harbin, China, Aug. 2019, pp. 1–6.

[18] S. Wu, C. Tian, W. Zhao, J. Zhou, and X. Zhang, "Design and analysis of an integrated modular motor drive for more electric aircraft," *IEEE Trans. Transport. Electrific.*, vol. 6, no. 4, pp. 1412–1420, Dec. 2020.

[19] Y. Fan, R. Cui, and A. Zhang, "Torque ripple minimization for inter-turn short-circuit fault based on open-winding five phase FTFSCW-IPM motor for electric vehicle application," *IEEE Trans. Veh. Technol.*, vol. 69, no. 1, pp. 282–292, Jan. 2020.

[20] F. Scuiller, F. Becker, H. Zahr, and E. Semail, "Design of a bi-harmonic 7-phase PM machine with tooth-concentrated winding," *IEEE Trans. Energy Convers.*, vol. 35, no. 3, pp. 1567–1576, Sep. 2020.

[21] J. Huang, P. Zheng, Y. Sui, J. Zheng, Z. Yin, and L. Cheng, "Third harmonic current injection in different operating stages of five-phase PMSM with hybrid single/double layer fractional-slot concentrated winding," *IEEE Access*, vol. 9, pp. 15670–15685, 2021.

[22] B. Zhao, J. Gong, T. Tong, Y. Xu, E. Semail, N.-K. Nguyen, and F. Gillon, "A novel five-phase fractional slot concentrated winding with low space harmonic contents," *IEEE Trans. Magn.*, vol. 57, no. 6, pp. 1–5, Jun. 2021.

[23] J. Huang, Y. Hao, Y. Sui, Z. Yin, L. Cheng, and P. Zheng, "Compensation strategy based on rotating rhombus method for five-phase PMSM with one-phase terminal short-circuit fault," *IEEE Trans. Magn.*, vol. 57, no. 6, pp. 1–5, Jun. 2021.

[24] Z. Yin, Y. Sui, P. Zheng, S. Yang, Z. Zheng, and J. Huang, "Short-circuit fault-tolerant control without constraint on D-axis armature magnetomotive force for five-phase PMSM," *IEEE Trans. Ind. Electron.*, early access, Jun. 3, 2021, doi: 10.1109/TIE.2021.3084172.

[25] Z. Gao, C. Cecati, and S. X. Ding, "A survey of fault diagnosis and fault-tolerant techniques—Part I: Fault diagnosis with model-based and signal-based approaches," *IEEE Trans. Ind. Electron.*, vol. 62, no. 6, pp. 3757–3767, Jun. 2015.

[26] Z. Gao, C. Cecati, and S. Ding, "A survey of fault diagnosis and fault-tolerant techniques—Part II: Fault diagnosis with knowledge-based and hybrid/active approaches," *IEEE Trans. Ind. Electron.*, vol. 62, no. 6, pp. 3757–3767, Apr. 2015.
[27] Z. Q. Zhu, D. Liang, and K. Liu, "Online parameter estimation for permanent magnet synchronous machines: An overview," *IEEE Access*, vol. 9, pp. 59059–59084, 2021.
[28] I. Abdennadher and A. Masmoudi, "Armature design of low-voltage FSPMSMs: An attempt to enhance the open-circuit fault tolerance capabilities," *IEEE Trans. Ind. Appl.*, vol. 51, no. 6, pp. 4392–4403, Nov. 2015.
[29] E. Haouas, I. Abdennadher, and A. Masmoudi, "Multi-phase fractional-slot PM synchronous machines with enhanced open-circuit fault-tolerance: Viable candidates for automotive applications," *World Electr. Vehicle J.*, vol. 12, no. 32, pp. 2–19, 2021.
[30] A. Masmoudi, *Design and Electromagnetic Feature Analysis of AC Rotating Machines*. Singapore: Springer, 2019.
[31] A. Masmoudi and A. Masmoudi, "3-D analytical model with the end effect dedicated to the prediction of PM eddy-current loss in FSPMMs," *IEEE Trans. Magn.*, vol. 51, no. 4, pp. 1–11, Apr. 2015.
[32] Q. Chen, D. Liang, S. Jia, and X. Wan, "Analysis of multi-phase and multi-layer factional-slot concentrated-winding on PM eddy current loss considering axial segmentation and load operation," *IEEE Trans. Magn.*, vol. 54, pp. 1–6, 2018.
[33] Y. Wang, Z.-Q. Zhu, J. Feng, S. Guo, Y. Li, and Y. Wang, "Rotor stress analysis of high-speed permanent magnet machines with segmented magnets retained by carbon-fibre sleeve," *IEEE Trans. Energy Convers.*, vol. 36, no. 2, pp. 971–983, Jun. 2021.

AHMED MASMOUDI (Senior Member, IEEE) received the B.S. degree from Sfax Engineering National School (SENS), University of Sfax, Sfax, Tunisia, in 1984, the Ph.D. degree from Pierre and Marie Curie University, Paris, France, in 1994, and the Habilitation degree (Postdoctoral Research) from SENS, in 2001, all in electrical engineering.

In 1988, he joined Tunisian University, where he held different positions involved in both education and research activities. He is currently a Full Professor of electric power engineering with SENS. He is also the Head of the Research Laboratory on Renewable Energies and Electric Vehicles and the Coordinator of the master on sustainable mobility actuators: research and technology. He is the author of more than 100 papers, 22 among which are published in IEEE TRANSACTIONS. He is the author or coauthor of four books and the co-inventor of U.S. patent. He has presented up to 11 keynote speeches in international conferences. His main research interests include the design of new topologies of ac machines and the implementation of advanced and efficient control strategies in drives and generators and applied to automotive as well as to renewable energy systems.

Prof. Masmoudi has been the Chairman of the Program and Publication Committee of the International Conference on Ecological Vehicles and Renewable Energie (EVER), annually-organized in Monaco, since 2007. He is the Head of the Founding Committee of the International Conference on Sustainable Mobility Applications, Renewables, and Technology (SMART) that has been organized at the Australian College of Kuwait, in 2015.

SAHAR MKAOUAR received the B.S. degree in electromechanical engineering from Sfax Engineering National School (SENS), University of Sfax, Sfax, Tunisia, in 2019, and the M.Sc. degree in sustainable mobility actuators: research and technology (SMART) from SENS, in 2021. She is currently pursuing the master's degree and defended her thesis with Kassel University, Kassel, Germany, within the Erasmus Exchange Program 20210607-ENIS-KA107.

Her current interests include the design, sizing, and optimization of permanent magnet machines dedicated to automotive and aerospace applications.

AICHA MAAOUI received the B.S. degree in electromechanical engineering from Sfax Engineering National School (SENS), University of Sfax, Sfax, Tunisia, in 2019, and the master's degree in sustainable mobility actuators: research and technology (SMART) from SENS, in 2020.

She is currently a Simulation, Modeling, and Support Engineer involved in motor design with Electro-Magnetic Works Inc., a golden partner of SOLIDWORKS.

MICHAEL SCHIER (Member, IEEE) received the Diploma and Ph.D. degrees in electrical engineering with specialization in energy technologies and electrical drives from the Technical University of Kaiserslautern, Germany.

From 1995 to 1999, he was involved in the development of electrical machines and power electronics for starter-alternators at the Department of Electric Vehicles, Siemens Company, in Würzburg, Germany. From 1999 to 2005, he was responsible for the development of blowers with electrical commutated motors and for automotive applications at Ebmpapst Company. Before his work at DLR, he was a Leader of power electronics development at Catem-Develec, a daughter company of Eberspächer Company. Since 2007, he has been working in the research area with the German Aerospace Center, Stuttgart, Germany, where he was first responsible for the development of alternative drives within the Institute of Vehicle Concepts. He is currently the Head of the Department of Vehicle Energy Concepts. The main topics of his scientific work were combined permanent magnet-electrically stator excited synchronous machines, starter-alternators for automotive application, electronically-commutated motors for axial and radial blowers, high-speed electric turbo-chargers, high torque machines for in-wheel motors for aircraft autonomous taxiing, and double motor systems with corresponding publications on international conferences.